Supporting Information for: Transient evolution of basal drag during glacier slip

Authors: Lucas Zoet[1*], Neal Iverson[2], Lauren Andrews[3], Christian Helanow[4]

1: Department of Geoscience, University of Wisconsin- Madison, Madison WI 53704, USA

2: Department of Geological and Atmospheric Sciences, Iowa State University, Ames, Iowa 50011, USA

3: Global Modeling and Assimilation Office, NASA Goddard Space Flight Center, Greenbelt MD 20771, USA

4: Department of Mathematics, Stockholm University, Stockholm, Sweden

Correspondence to: lzoet@wisc.edu

S1. Measurements of ice-chamber volume and final cavity geometry

Ice chamber expansion and contraction, associated with growth or shrinkage of cavities or melting of ice and drainage of meltwater, is measured using a vertically mounted LVDT (Figs. S1 & S3). The ice chamber is affixed to a crossmember that rises and falls as the ice chamber contracts and expands, respectively. Two arms that extend horizontally from the cross member are in contact with two vertical I-beams, prohibiting the ice chamber from rotating with the upper platen (Fig. S3). The crossmember arms are in contact with the vertical I-beams through a set of bearings that transfer the torque load but allow the vertical position of the ice chamber to change with minimal resistance. The LVDT is placed as close as possible to the central axis of the ice chamber, with the plunger of the LVDT in contact with the baseplate that supports the chamber at its bottom (Fig. S1). The construction of the crossmember minimizes tilting. Furthermore, the placement of the LVDT near the central axis (Fig. S1) further reduces the effects of any off-axis tilt. The LVDT is an RDP Group, model number LDC500A, which has a maximum range of ±12.5 mm and a maximum deviation of 12.5 microns over the full range. The LVDT's plunger is spring-loaded, accommodating of both expansion and contraction within its design range. In these experiments cavity growth drives ice chamber expansion, and melting of ice drives ice chamber contraction. Due primarily to melting of the ice, the LVDT has to be occasionally re-zeroed manually, at which time the LVDT is physically shifted up to the zero position so that continued contraction of the sample chamber does not cause the baseplate to rise so far that it loses contact with the LVDT. The timeseries is manually shifted in MATLAB to account for any re-zeroing.

Cavities developed in the lees of the 12 sinusoidal bumps in these experiments, and as cavities expanded (or contracted), the ice chamber expanded (or contracted) accordingly. The ice chamber confines the sides of the ice ring and the upper platen is fixed vertically, so expansion caused by cavity growth lowers the ice chamber. Thus, although the shapes of cavities are not known during experiments, the lowering of the ice chamber, as measured by the LVDT, records the increase in total cavity volume per unit area of the bed.

To determine the shapes of the cavities at the ends of experiments, a custom-made jig is used to measure the geometry of the ice-ring sole (Fig. S2). Following an experiment, the upper platen is detached and retracted from the ice ring, which remains in the ice chamber. A set of four ice screws is used with a winch system to extract the ice ring from the chamber. The freezer is then set to -10 ºC to halt melting of the ice ring. It is flipped over so its sole is facing up and allowed to cool for 24-48 hr before the jig is used. The jig is a clear acrylic table with holes every 1.3˚ along five separate arcs spaced evenly across the centermost 80% of the width of the ring (20 cm) (Fig. S2). A depth meter pressed again the ice-ring sole measures its vertical position relative to the jig to within 0.01 mm. The jig can measure ~1/6 of the circumference of the ice ring at one placement, so the jig must be incrementally repositioned around the ring to fully reconstruct the ice sole morphology. The data are digitized to construct the 3D morphology of the base of the ice ring (Fig. 4). This morphology, together with the morphology of the sinusoidal bed, provide the final cavity size and shape from an experiment. See Petersen (2012) for more details.

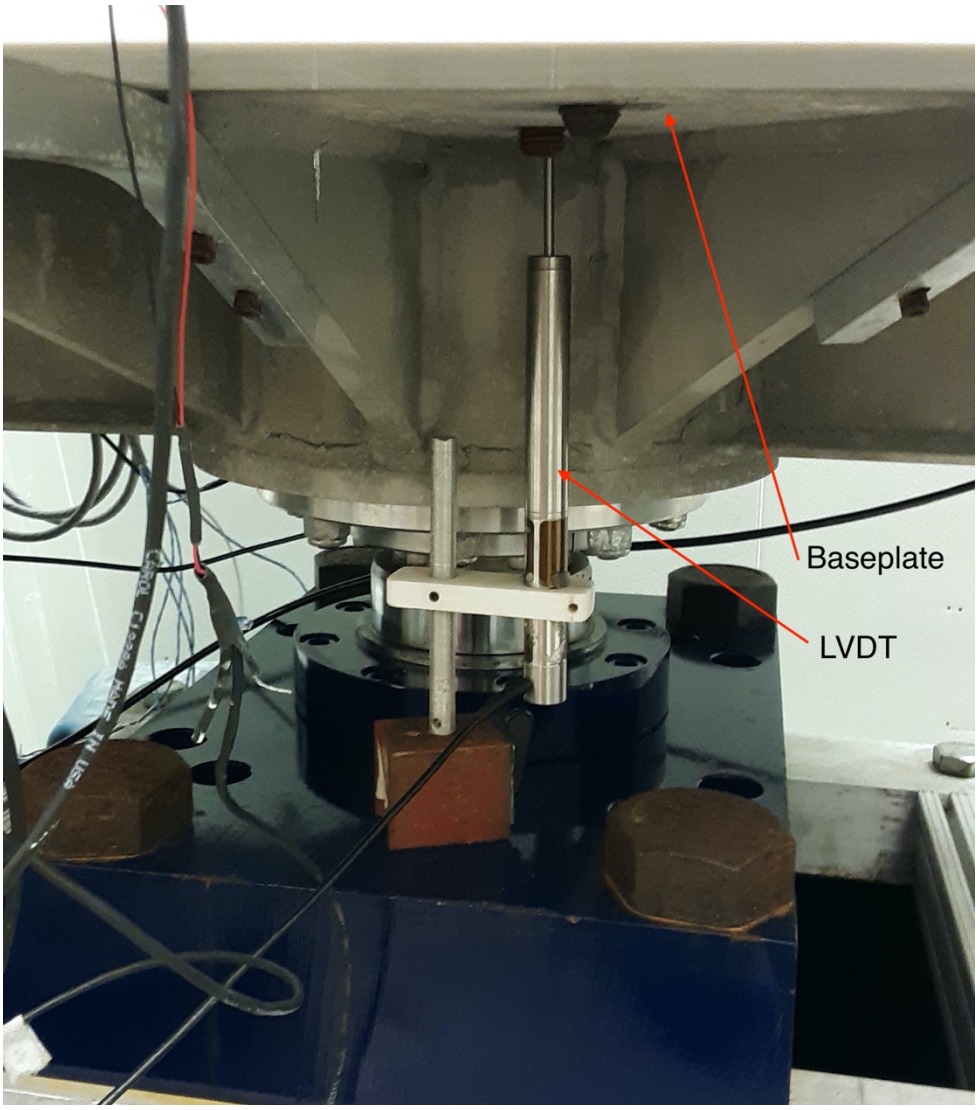

Fig S1. LVDT location. The LVDT is installed vertically and normal to the baseplate that supports the ice chamber (Fig. S3) and moves up or down with it. As the ice chamber moves up and down, the LVDT's spring loaded plunger is pushed out or in. The body of the LVDT is fixed.

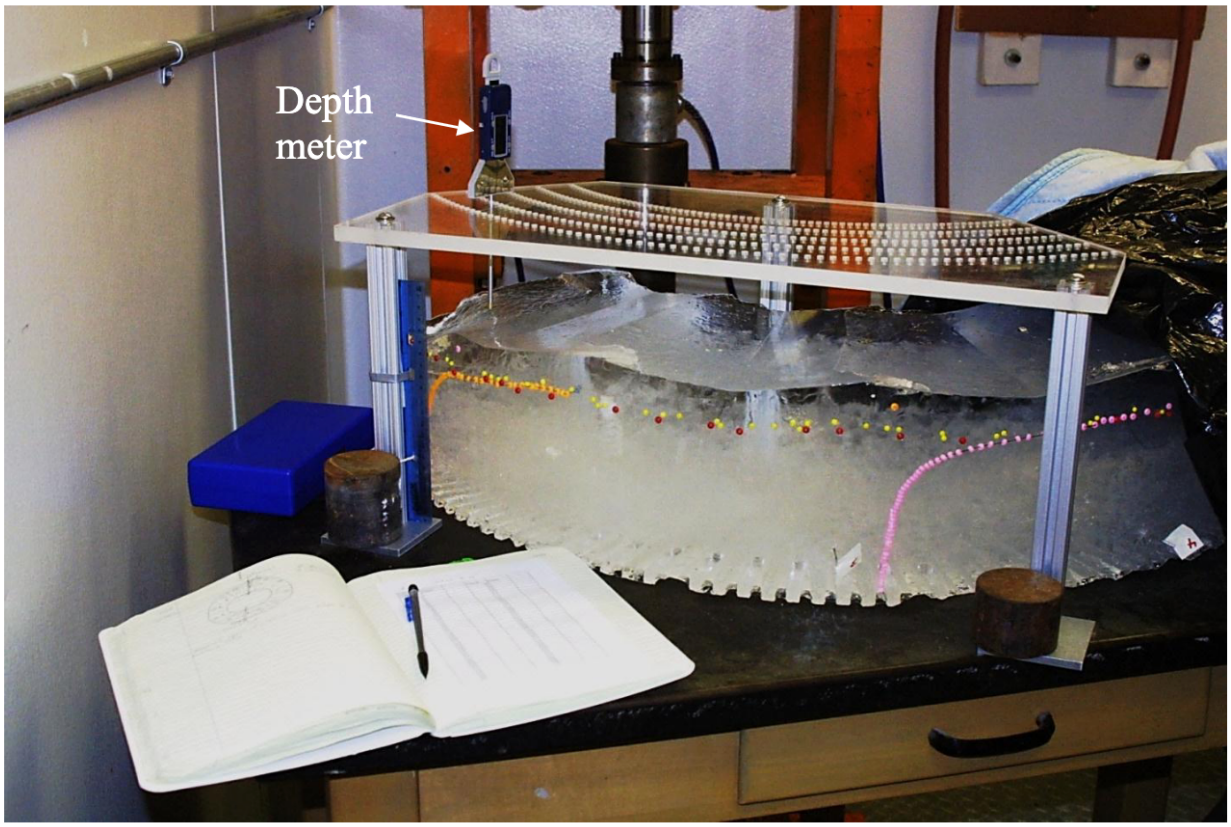

Fig S2. Ice-sole jig. An inverted ice ring with the clear acrylic jig set atop it. The depth meter is used to measure the distance between the jig's upper surface and the upward-facing sole of the ice ring (from Petersen, 2012).

S2. Double-valued, steady-state drag

To estimate the steady-state, double-valued drag relation, we replicate the method used by Zoet and Iverson (2015) that successfully fit their experimental results. Steady cavity geometries are estimated using the model of Kamb (1987), which balances the closure rate of cavities by ice creep with their opening by sliding. From the cavity geometry, the steady drag is estimated from Lliboutry (1968; 1979).

For the case of a cavity in the lee of an isolated step, Kamb determined the cavity height *g(x)* as a function of the bump height, *h*, and cavity length, *l*, where *x* is the distance downstream from the step riser along the horizontal bed:

$$g(x) = h\left(\frac{1}{2} - \frac{1}{\pi}\sin^{-1}\frac{2x-l}{l} - \frac{2(2x-l)\sqrt{x(l-x)}}{\pi l^2}\right), \tag{A1}$$

where $0<x<l$. Kamb determined the cavity length for the case of a linear-viscous rheology but suggested an approximation for the power-law rheology of ice. For the case of negligible melting of cavity roofs by water—applicable to the experimental results—the approximation is

$$l = \sqrt{\frac{8vh}{\pi}\left(\frac{B}{N}\right)^n}, \tag{A2}$$

where v is the sliding speed, N is the effective pressure, B is the viscosity parameter of Glen's power-law flow rule for ice creep, with stress exponent, n (Iverson and Petersen, 2011). Equations A3 and A4 are used to estimate cavity geometry for the sinusoidal bed of the experiment by considering h to be twice the amplitude of the sinusoid and extending the cavity roof as predicted by equation A3 until it is truncated by the ascending limb of the sinusoid immediately downstream. Parameter values from the experiment are h=30.6 mm and N=500 kPa, with n=3 (Cuffey and Patterson, 2010), and B=6.3x10^7 Pa s$^{1/3}$, a value that optimizes the fit of equation A1 to measured cavity roofs and is close to the value advocated for clean, glacier ice at its PMT (B=7.5 x10^7 Pa s$^{1/3}$, Cuffey and Paterson, 2010).

The drag is estimated from Lliboutry (1968; 1979). For a sinusoid of angular frequency (i.e., wavenumber), $\omega=2\pi/\lambda$, and in a direction, x, parallel to the regional bed slope, the bed shear stress (drag force per unit bed area), τ, is

$$\tau = \frac{a\omega}{2} N\Phi \tag{A3}$$

(Lliboutry, 1979, equation 88, therein). N is equal to the effective pressure of the experiments, and Φ is a coefficient dependent on the fraction, s, of the bed in contact with ice and on the position, x_c, where ice separates from the bed:

$$\Phi = \frac{[\pi s - \frac{1}{2}\sin(2\pi s)]\sin(\pi s - \omega x_c)}{\sin(\pi s) - \pi s\cos(\pi s)}, \tag{A4}$$

with x_c obtained from

$$x_c = \frac{1}{\omega}\cot^{-1}\left(\frac{2\pi(1-s)+\sin(2\pi s)}{1-\cos(2\pi s)}\right) \tag{A5}$$

(Lliboutry, 1968, modified from equations 14 and 9, respectively, therein). We estimate, s, in these equations as a function of sliding speed using the theory of Kamb (1987), as described in equations A1 and A2.

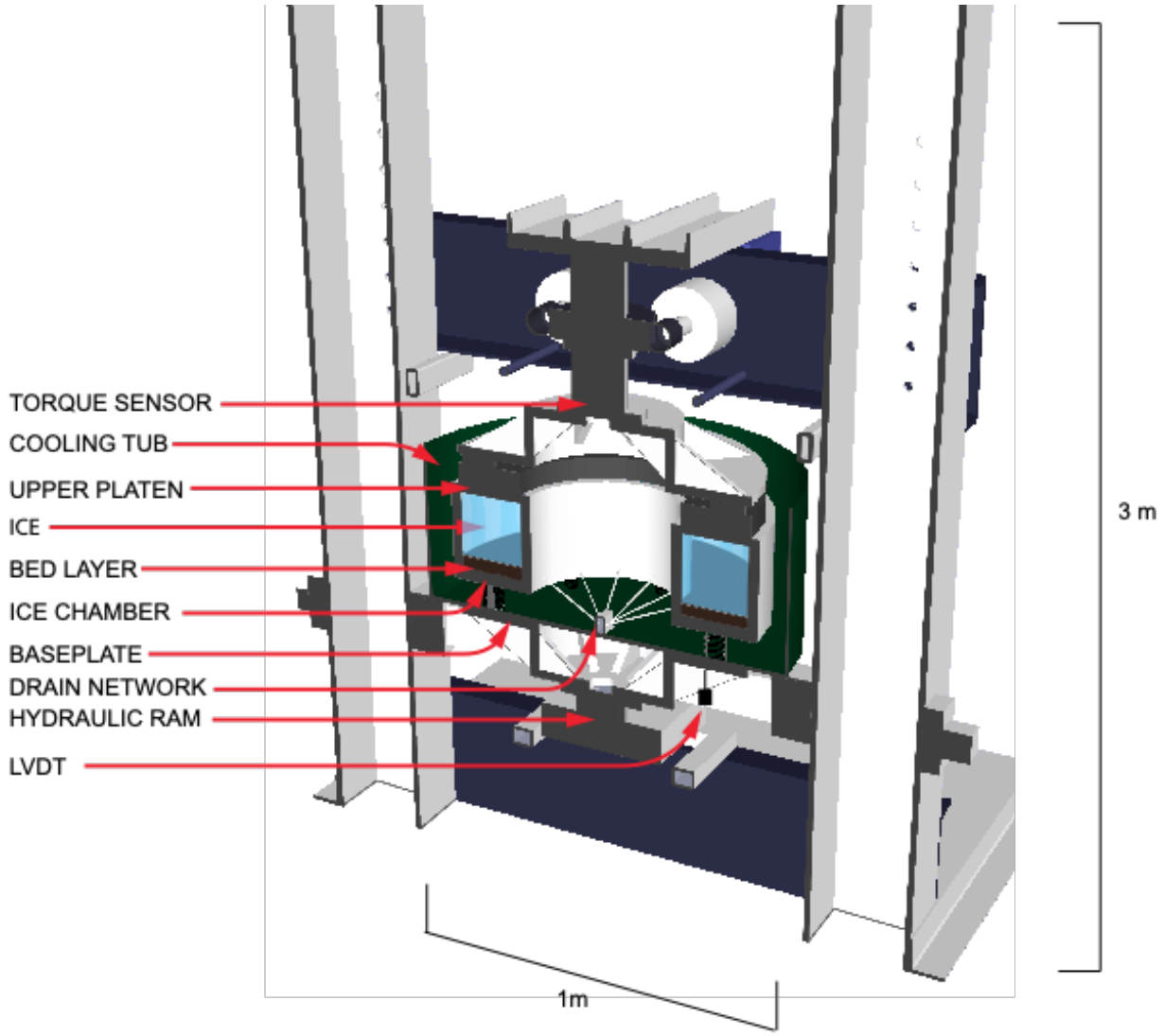

Fig S3. Schematic of the Iowa State University ring-shear device. This device is housed in a cold room. Note the torque sensor used to measure drag and the LVDT used to measure sample-chamber contraction or expansion.

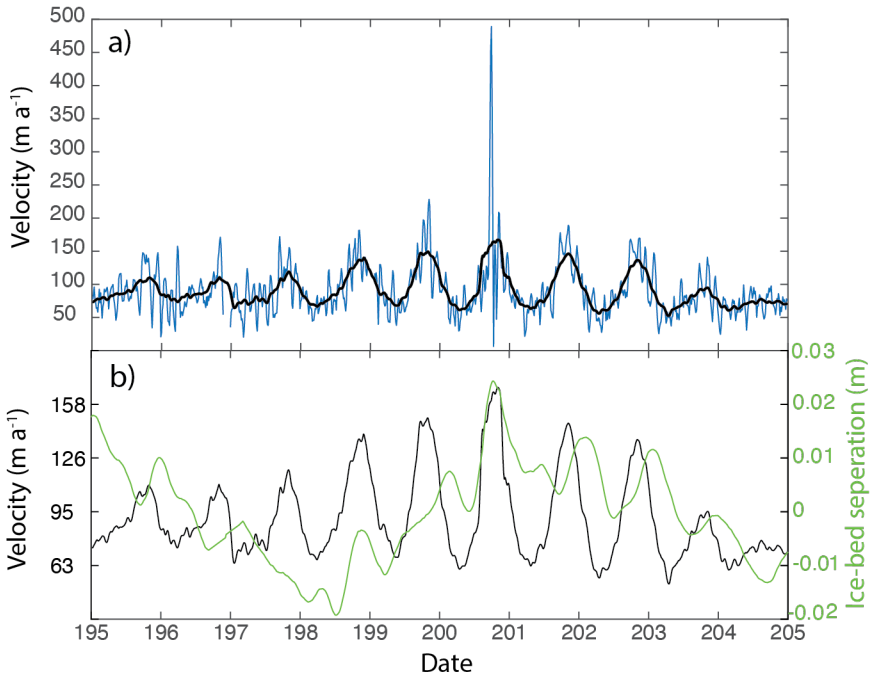

Fig S4. Field data from the GIS. a) Raw velocity data (blue) recorded at the FOXX site for 10 days in 2012. The data have been smoothed with a 450-minute moving-average window (black line) to remove erratic data. b) Smoothed velocity (black) compared with the field proxy for ice-bed separation (green).

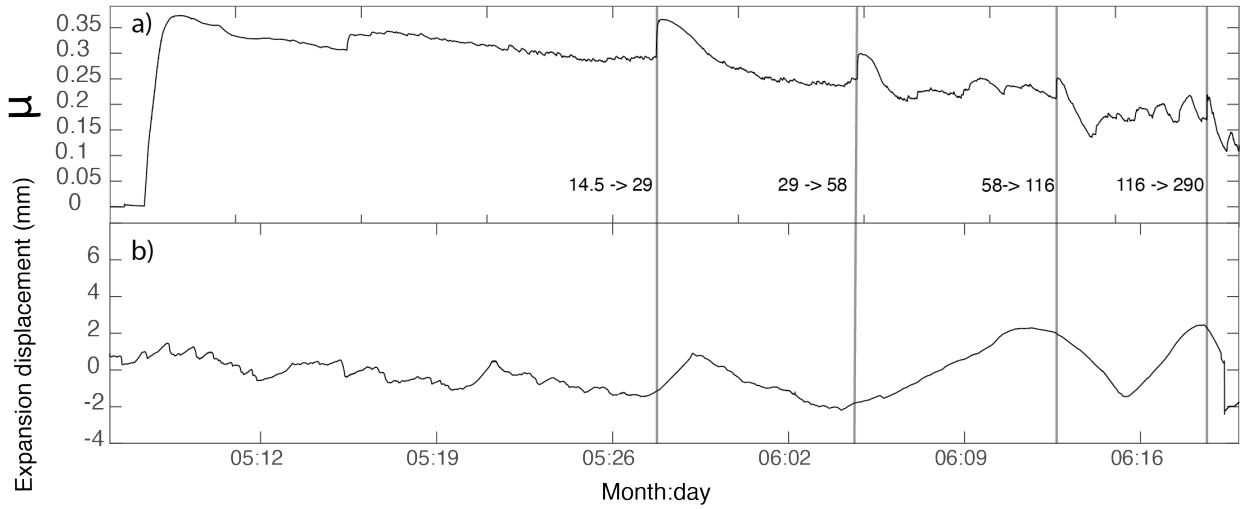

Fig S5. Full experimental time series. a) Evolution of friction for the full experimental duration. The vertical lines are the times when the velocity was stepped. The values on the plot are the velocity steps in m a^{-1}. b) Chamber expansion and contraction mainly from cavity growth and shrinkage. Expansion occurs when values become larger. LVDT measurements were detrended with a single value to remove most of the background thinning due to melting of the ice ring but some component still remains. In Fig. 6 more accurate time dependent melt rates were removed than in this figure. Note there was a power failure around day 5:15 which accounts for the small step in μ at that time.

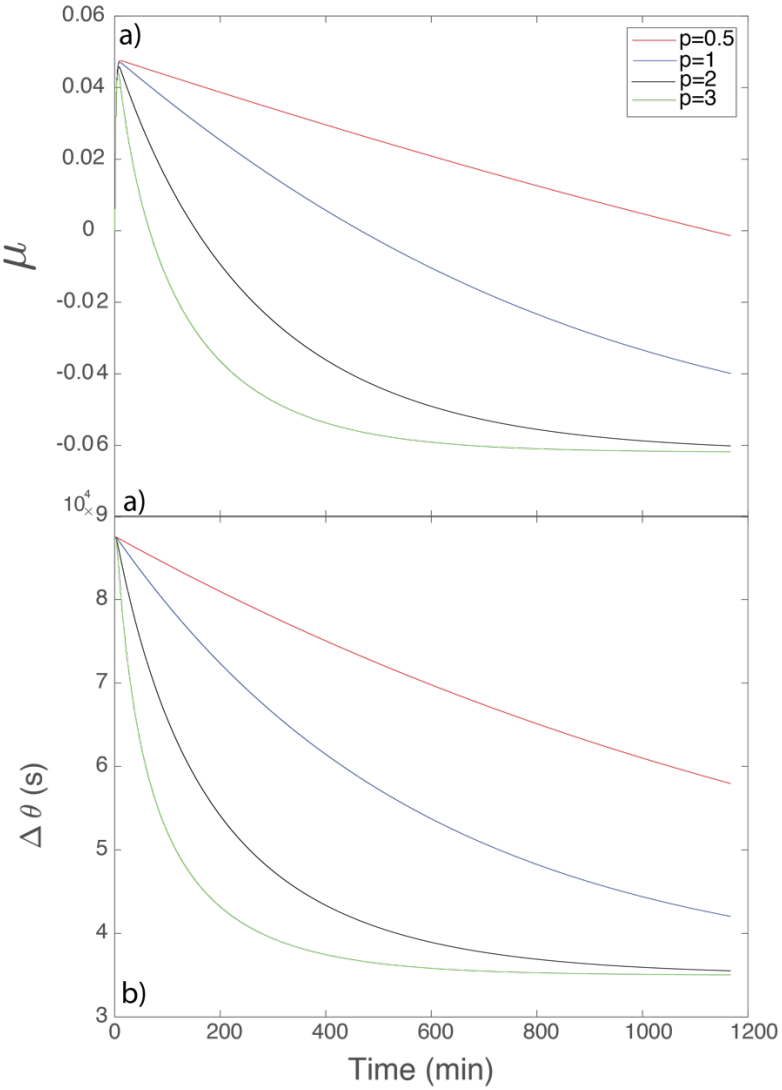

Fig S6. Friction and state evolution of the final velocity step 116 →290 m a^{-1} for four different p values in equation 2. a) The upper panel reflects the evolution of the friction with time for different values of the p exponents. b) The state variable reflects the evolution of the ice-bed contact area through time. Note the more nonlinear response as the exponent is increased. The value p=1 fit the experimental measurements best (Fig. 5).

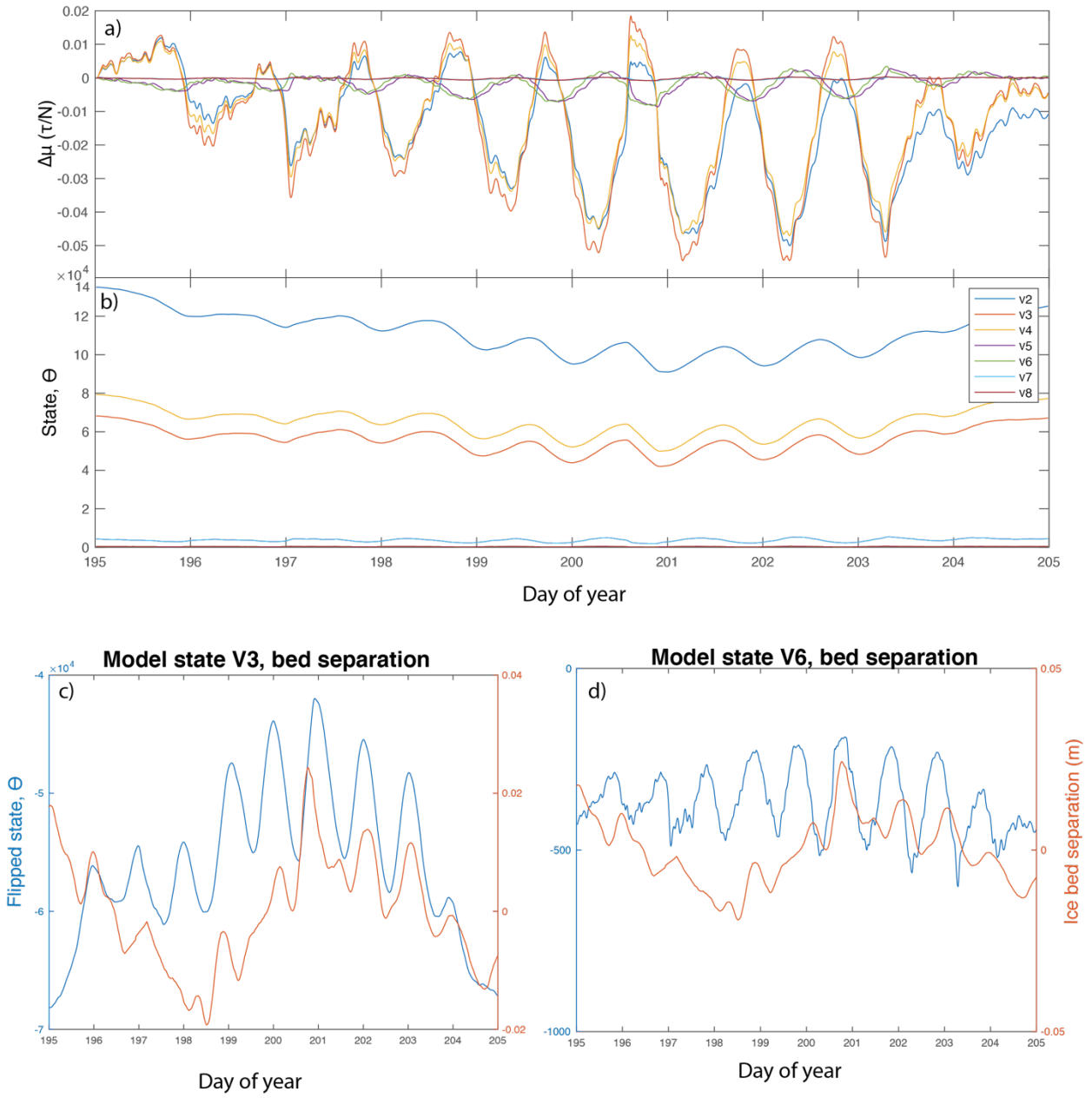

Fig S7. RSF model results driven with surface velocity observations and employing the different sets of RSF parameters shown in Table S1. Model runs V2-V4 were based on values recorded in these experiments. Values used in V5-V8 represent much smaller magnitude and shorter duration transients and are loosely based on observations from Zoet and others, (2013) which did not include cavitation. a) Friction response for different model runs. The largest difference between outcomes occurs between run group V2-V4 and run group V5-V8 where D_c values were significantly smaller. The smaller D_c in effect reduces the time (or slip distance) required for cavities to adjust to the new steady state. This change has a significant effect on the phasing and magnitude of the friction response. b) State evolution for the various model runs. c) State evolution for V3 compared with the measured ice-bed separation. d) Modeled state evolution for V6 compared with the measured ice-bed separation. The model runs with larger D_c values (V2-V4) have a phasing of

θ that agrees best with the observed ice-bed separation (i.e., c vs d). This agreement suggests that those model runs (V2-V4) may better represent the subglacial effects from cavitation than V5-V8, indicating that their frictional response is more likely to be useful as well. Within the V2-V4 group, V2 best represents the phasing of the ice-bed separation observed and hence these parameters were used to drive the model in the remainder of the study.

Table S1. RSF model parameters

Run	a [-]	b [-]	D_c [cm]
V2	0.052	0.120	31.5
V3	0.071	0.127	15.9
V4	0.058	0.11	18.5
V5	0.01	0.02	1
V6	0.01	0.02	0.1
V7	0.001	0.002	1
V8	0.001	0.002	0.1

References

Cuffey, K. M., & Paterson, W. S. B. (2010). *The physics of glaciers*. Academic Press.

Iverson, N. R., and Petersen, B. B. (2011). A new laboratory device for study of subglacial processes: first results on ice–bed separation during sliding. *Journal of Glaciology*, *57*(206), 1135-1146.

Kamb, B. (1987) Glacier surge mechanism based on linked cavity configuration of the basal water conduit system. *Journal of Geophysical Research: Solid Earth*, *92*(B9), 9083-9100.

Lliboutry, L. (1968) General theory of subglacial cavitation and sliding of temperate glaciers. *Journal of Glaciology*, *7*(49), 21-58.

Lliboutry, L. (1979). Local friction laws for glaciers: a critical review and new openings. *Journal of Glaciology*, *23*(89), 67-95.

Petersen, B. B. (2012). *An experimental study of ice-bed separation during glacial sliding.* Masters dissertation, Iowa State University.

Zoet, L. K., Carpenter, B., Scuderi, M., Alley, R. B., Anandakrishnan, S., Marone, C., and Jackson, M. (2013) The effects of entrained debris on the basal sliding stability of a glacier. *Journal of Geophysical Research: Earth Surface*, *118*(2), 656-666.

Zoet, L. K., and Iverson, N. R. (2015) Experimental determination of a double-valued drag relationship for glacier sliding. *Journal of Glaciology*, *61*(225), 1-7.